Extreme Weather exacerbates Ozone Pollution in the Pearl River Delta, China: Role of Natural Processes

Nan Wang[1], Hongyue Wang[2], Xin Huang[3], Xi Chen[4], Yu Zou[5], Tao Deng[5], Tingyuan Li[6], Xiaopu Lyu[7*], Fumo Yang[1*]

[1]College of Carbon Neutrality Future Technology, Sichuan University, Sichuan, China
[2]Department of Atmospheric Science, China University of Geosciences, Wuhan, 430078, China
[3]School of Atmospheric Science, Nanjing University, Nanjing, China
[4]Institute of Mass Spectrometry and Atmospheric Environment, Guangdong Provincial Engineering Research Center for On-line Source Apportionment System of Air Pollution, Jinan University, Guangzhou, PR China
[5]Institute of Tropical and Marine Meteorology, China Meteorological Administration (CMA), Guangzhou, China
[6]Guangdong Ecological Meteorological Center, Guangzhou, China
[7]Department of Geography, Hong Kong Baptist University, Hong Kong, 000000, China

*Correspondence to xiaopu_lyu@hkbu.edu.hk and fmyang@scu.edu.cn

KEYWORDS: ozone pollution, extreme weather, natural process, BVOC emission, STE

Abstract

Ozone (O_3) pollution research and management in China have mainly focused on anthropogenic emissions, while the importance of natural processes is often overlooked. With the increasing frequency of extreme weather events, the role of natural processes in exacerbating O_3 pollution is gaining attention. In September 2022, the Pearl River Delta (PRD) in South China experienced an extended period (25 days) of regional O_3 exceedances and high temperatures (2nd highest over last 2 decades) due to extreme weather conditions influenced by the Subtropical High and typhoon peripheries. Employing an integrated approach involving field measurements, machine learning, and numerical model simulations, we investigated the impact of weather-induced natural processes on O_3 pollution by considering meteorological factors, natural emissions, chemistry pathways, and atmospheric transport. The hot weather intensified the emission of biogenic volatile organic compounds (BVOC) by ~10%. Isoprene and biogenic formaldehyde accounted for 47% of the in-situ O_3 production, underscoring the predominant role of BVOC emissions in natural processes. The chemical pathway of isoprene contributing to O_3 formation was further explored, with O_3 production more attributable to the further degradation of early generation isoprene oxidation products (contributed 64.5%) than the direct isoprene oxidation itself (contributed 35.5%). Besides, it was found that the hot weather significantly promoted regional photochemical reactions, with meteorological factors contributing to an additional 10.8 ppb of O_3 levels compared to normal conditions. Temperature was identified as the dominant meteorological factor. Furthermore, the typhoon nearing landfall significantly enhanced the cross-regional transport of O_3 from northern to southern China through stratosphere-to-troposphere exchange (STE). The CAM-Chem model simulations revealed that the STE-induced O_3 on the PRD surface could reach a maximum of ~ 8 ppb, highlighting the non-negligible impact of STE. This study highlights the importance of natural processes exacerbated by extreme weather events in O_3 pollution and provides valuable insights for O_3 pollution control under global warming.

1 Introduction

Ground-level ozone (O_3) is a secondary air pollutant with adverse effects on human health, vegetation, crop yields, and climate (Knowlton et al., 2004; Ashmore, 2005; Eyring et al., 2013). The formation of tropospheric O_3 is a result of sunlight-driven photochemical reactions involving nitrogen oxides (NO_x), volatile organic compounds (VOC), and other pollutants (Derwent et al., 1998; Jacob, 2000). The relationship between O_3 and its precursors exhibits a non-linear pattern that varies across different regions (Jenkin and Clemitshaw, 2000). O_3 and its precursors originate from both anthropogenic activities and natural processes such as fossil fuel combustion, biogenic volatile compound (BVOC) emissions and stratosphere-troposphere exchange (STE). Meteorological conditions also play a crucial role in influencing O_3 pollution, adding complexity to mitigation efforts (Wang et al., 2017).

Since the industrial revolution, the northern hemisphere has experienced a significant increase in O_3 pollution, particularly in mid-latitude cities with large populations and industries (Gaudel et al., 2018). In recent decades, Europe and the United States have made notable progress in mitigating O_3 pollution through emission control efforts. However, eastern Asia, notably China, continues to face a severe O_3 pollution problem (Lyu et al., 2023). Despite the implementation of strict emission control measures, such as the Air Pollution Prevention and Control Action Plan and the reduction in fine particulate matter concentrations, O_3 levels in China have continued to rise (Wang et al., 2019). Lu et al. (2018) reported that O_3 pollution days in China are 93 to 575% higher compared to other developed countries, indicating the significant public concern surrounding this issue.

Despite human activities being recognized as major contributors to severe O_3 pollution, it is also important to acknowledge the role of meteorological conditions on the dynamics of tropospheric O_3 concentrations. For example, temperature has a direct impact on chemical reaction rates involved in O_3 formation as well as the emissions of BVOC from vegetation (Lu et al., 2019). Atmospheric water vapor, on the other hand, plays a crucial role by providing hydrogen oxide (HO_x) radicals and directly influencing O_3 photochemistry (Camalier et al., 2007). Additionally, wind patterns

contribute to the transport and dispersion of pollutants, thereby influencing the spatial distribution of O_3 and its precursors (Wang et al., 2022). Nonetheless, the local meteorological parameters are controlled by synoptic weather system. Generally, the role of weather systems manifests in two aspects, one is via the influence on the regional transport of pollutants, and the other is modulating the aggregation and dispersion of local air pollutants (Ding et al., 2017). Extensive research conducted in eastern China has shed light on the importance of weather patterns and addressed on the impact of extreme weather contributing to O_3 pollution. Notably, anticyclones (such as high-pressure systems) and the periphery of typhoons have emerged as prominent factors (Chan and Chan, 2000; Han et al., 2020; Gao et al., 2021). Besides, natural processes, including the natural sources, chemistry and atmospheric transport of O_3, are highly meteorology-sensitive and might further aggravate O_3 pollution under extreme weather. For example, the wildfire caused by hot and dry weather could emit large amount of carbon monoxide (CO), NO_x and VOCs and exacerbate O_3 pollution (Westerling et al., 2006; Yue and Unger, 2018; Lei et al., 2022); vegetation-released BVOC emissions are sensitive to temperature and have been proven to increase during hot season and thus accelerate urban O_3 formation (Pusede et al., 2015; Wang et al., 2022); an STE event would bring stratospheric O_3 to the troposphere under a large-scale/mesoscale process such as tropopause folds, gravity wave breaking, and deep convections (Stohl et al., 2003; Wang et al., 2020). As global warming progresses, there is an increase in the frequency of extreme weather events which further impact surface O_3 (Banerjee et al., 2016; Lu et al., 2019). These impacts may undermine or offset the efforts by anthropogenic emission reductions, posing risks to the ecological environment. Therefore, understanding the influence of natural process on the formation of ground-level O_3 is essential for gaining insights into the dynamics of O_3 pollution and developing effective strategies for managing air quality.

The Pearl River Delta (PRD) region, known for its high levels of anthropogenic emissions and surrounded by significant vegetation cover, frequently suffers from extreme weather events such as heat waves and

tropical cyclones. The PRD region has emerged as a typical hotspot witnessing an increase in O_3 pollution, making it an ideal location to investigate the impact of extreme weather on O_3 pollution. In September 2022, the PRD endured a prolonged period of hot weather, leading to more than 20 days of regional O_3 exceedance. Here, by integrating simultaneous measurements, machine learning, and numerical model simulations, we aim to improve the understanding of how natural processes induced by extreme weather events affecting O_3 pollution and provide new insights for future O_3 pollution control efforts.

2 Methods and Materials

2.1 Data Source

In-situ observations were conducted at the Guangzhou Haizhu Urban Ecological Meteorological Comprehensive Observation Base (HZ Base, 23°05'N, 113°22'E), which is located in the North area of the Guangzhou Haizhu District National Wetland Park (as shown in Fig. 1(a)). The observation base is surrounded by basic farmland protection areas and represents a typical composite wetland system consisting of river channels, creeks, fruit orchards, and the Jiangxinzhou Island. It also encompasses commercial streets, residential areas, and major transportation routes, providing a representation of wetland climate and human activities. Synchronous online observations of O_3, NO_x, SO_2, CO, components of VOCs, and meteorological parameters (surface winds, temperature, relatively humidity, precipitation and solar radiation) were carried out at this observation base. All the data are collected at the HZ Base from Sept. 1st to Sept. 30th, with a time resolution of 1 hour. Detailed information about the data used, including the monitoring instruments, data coverage, and access method, was summarized in Table S1. Briefly, ambient concentrations of O_3, NO_x, CO and SO_2 were routinely measured using instruments produced by Thermo Scientific (49i-D1NAA, 42i-DNMSDAA, 48i-DNSAA and 43i-DNSAA, respectively). The species of VOC components were monitored by GC5000 analysis systems coupled with flame ionization detectors (FID) from AMA Instruments GmbH (AMA, Germany). The target compounds of the instrument were the 56 VOCs designated as photochemical precursors by the US Environmental

 All instruments were regularly calibrated and maintained for different durations. Meteorological data, including temperature, solar radiation, precipitation, relative humidity and winds, were obtained at the same site from the China Meteorological Administration. The in-situ measurements were mainly used to drive a photochemical box model as described below. Additionally, the air quality monitoring network established by the Ministry of Ecology and Environment of China was utilized to identify O_3 pollution event in PRD. There were 56 monitoring sites distributed in the whole region (Fig. 1(a)) and the 90th percentile of the maximum daily 8-hour average (MDA8-90) O_3 concentration was employed to assess the regional degree of O_3 pollution. A regional O_3 exceedance occurs when the MDA8-90 exceeds the China's Grade II standard (i.e., 160 μg/m^3).

In addition to the in-situ data, ancillary data from the fifth generation of the European Centre for Medium-Range Weather Forecasts atmospheric reanalysis (ERA5) were utilized. The ERA5 data, at a resolution of 0.25° × 0.25° grid, corresponded to the same time period and interval as the observed data and provided information such as boundary layer height, potential vorticity, vertical velocity, geopotential height, specific humidity and O_3 mass mixing ratio. Besides, typhoon tracks occurred in West Pacific Ocean were collected from China Meteorology Administration Tropical Cyclone Data Center (https://tcdata.typhoon.org.cn).

2.2 Stepwise Regression Analysis

The stepwise regression analysis, as a common method of machine learning, was used to simulate the dynamics of O_3 concentrations and quantitatively assess the influence of various meteorological factors on pollutant variations. The method was designed to construct an optimal equation by iteratively selecting significant factors while eliminating non-significant ones to address autocorrelation concerns (Johnsson, 1992). In this study, simple regressions were firstly performed for each explanatory variable, and the variable with the most significant contribution was

identified. Subsequently, additional variables were gradually introduced, and the F-test and t-test were employed to evaluate their significance. Non-significant variables were progressively eliminated until we obtained a final set of critical explanatory variables. Following variable selection, a multivariate linear regression equation was established to capture the variation of O_3 concentrations:

$$O_3(t) = \alpha VAR_1(t) + \beta VAR_2(t) + \gamma VAR_3(t) + \cdots + \eta VAR_n(t) + R(t) \quad (1)$$

In Eq. (1), $O_3(t)$ represents the temporal changes in O_3 concentration at hour t. The coefficients (α, β, γ, η) for each variable (VAR) were determined during the stepwise regression process, while R(t) represents the residual error term. This approach enables us to effectively analyze the intricate relationship between meteorological factors and O_3 concentrations, providing valuable insights into the dynamics of O_3 pollution. This utilized approach has proven effective in our previous pollutant simulations (Chen et al., 2022). In this study, the model's performance was validated through Fig. S1, demonstrating a strong correlation (Pearson correlation coefficient (R) = 0.84 and p-Value (from two-tailed t-test) < 0.01) between the observed and simulated O_3 concentrations.

2.3 Lagrangian Dispersion Modeling

We conducted backward Lagrangian particulate dispersion modeling (LPDM) using the Hybrid Single-Particulate Lagrangian Integrated Trajectory model (HYSPLIT, https://www.arl.noaa.gov/hysplit/, last access: Nov. 15, 2023) to identify the dominant air flow impacting the receptor area. The meteorology fields were from the Global Data Assimilation System (GDAS) data. In this study, we released 3000 particulates at 100 m above sea level (a.s.l) over the site (HZ Base) and tracked their backward movement for 48 hours with a time resolution of 1 hour. The positions of the particulates were determined using both vertical and horizontal calculations, considering mean wind and turbulence transport. The model finally identified the "retroplume" footprint representing the spatial residence time of the particulates and could be regarded as the distribution of the simulated air mass's surface probability or residence time.

2.4 MEGAN model

The Model of Emissions of Gases and Aerosols from Nature (MEGAN, version 2.1, available at: https://bai.ess.uci.edu/megan/, last access Nov. 15, 2023) was used to estimate BVOC emissions from terrestrial ecosystems (Guenther et al., 2012). The model could calculate 147 individual biogenic compounds and lump them into the appropriate VOC mechanisms such as CB05, RACM, SAPRC99 and etc. Herein, the CB05 mechanism was adopted for VOC treatment. Due to the versatility and compatibility, the MEGAN model could be incorporated into many widely used chemical transport models with horizontal resolution ranging from a few kilometers to several hundred kilometers. In this study, the plant function type (PFT) data was from Moderate-Resolution Imaging Spectroradiometer (MODIS) MCD12Q1 product and the leaf area index (LAI) data was from MODIS MCD15A2H product. The input meteorology including temperature, solar radiation, and relative humidity was obtained from Weather Research Forecast-Community Multi Scale Air Quality (WRF-CMAQ) simulations with a horizontal resolution of 12km×12km. The configuration of WRF-CMAQ was summarized in Table S2. In particular, to emphasize the influence of extreme weather, comparisons of BVOC emissions from parallel simulations were conducted. In detail, we employed two sets of meteorological fields to drive the MEGAN model, respectively. One set was based on the WRF-simulated meteorology from September 2022, while the other utilized the average meteorological fields from the preceding three years (2019-2021).

2.5 In-situ photochemistry modeling

In-situ O_3 formation was simulated using the Framework for 0-D Atmospheric Modeling (F0AM) incorporating Master Chemical Mechanism v3.3.1 (https://sites.google.com/site/wolfegm/models, last access: Nov. 15, 2023). The application method was roughly in line with that in Lyu et al. (2022). Briefly, the model was constrained by observations including O_3, NO_x, CO, sulfur dioxide (SO_2), VOCs species and meteorological parameters collected at HZ Base at hourly resolution. Specifically, HCHO was not measured and was constrained by the WRF-CMAQ simulation results (The validation of WRF-CMAQ was

summarized in Table S3). A 'family conservation' that set the total NO_x to the observed value every hour and allowed nitrogen monoxide (NO) and nitrogen dioxide (NO_2) to evolve over time was applied. Photolysis frequency of NO_2 observed at HZ Base was input and used to correct the photolysis frequencies of other species. Net O_3 production rate (OPR) was calculated as the difference between O_3 production rate (NO_2 production through NO oxidation by peroxyl radicals) and destruction rate (NO_2 reacting with OH, O_3 photolysis, ozonolysis of alkenes, and O_3 consumption by OH and HO_2), in line with the way adopted in previous studies (Lyu et al., 2019; Wang et al., 2017). The reaction rates for a total of 17,224 reactions were extracted to diagnose the main isoprene-related pathways leading to O_3 formation.

2.6 CAM-Chem model

The CAM-Chem (Chemical Lagrangian Model of the Stratosphere), a component of the National Center for Atmospheric Research (NCAR) Community Earth System Model (CESM) version 2.2.0, was utilized to simulate the impact of STE transported O_3 on the troposphere. The meteorological fields were obtained from Model-Era Retrospective analysis for Research and Applications-Version 2 (MERRA-2) and regridded to a 32-vertical layer with a horizontal resolution of 0.9×1.25°. The chemistry mechanism employed was the Model for Ozone and Related Chemical Tracers (MOZART). Further information about the model can be found in the CAM-Chem Wiki (https://wiki.ucar.edu/display/camchem). To validate the model's performance, we compared the distribution of the simulated O_3 with O_3 from AIRS (Atmospheric Infrared Sounder). Both the monthly averaged distribution and an STE-induced O_3 intrusion case were compared (Fig. S2). Although the CAM-Chem simulations showed slightly higher O_3 levels in southern China, the correlation coefficient in Eastern China was 0.79 (passed a 95% significance test), indicating the CAM-Chem model relatively well produced O_3 at higher levels (Fig. S3). Besides, it was worth noting that the satellite retrievals themselves contain uncertainties, mainly from the impact of clouds, aerosols, surface albedo and the inversion algorithms (Briegleb et al., 1986; De Smedt et al., 2010; Povey and Grainger, 2015). Overall, the simulated O_3 showed good

agreement with the AIRS data in terms of magnitude and spatial pattern, indicating satisfactory model performances. Furthermore, a comparison of the CAM-Chem simulated ground-level O_3 with the surface network monitoring was also conducted (Fig. S4). The daily magnitude and variation trend were successfully captured in Guangzhou, with a mean bias error (MBE) of -7.9 ppb and a root mean square error (RMSE) of 16.3 ppb. This demonstrated a good reproduction of surface O_3 concentrations. Indeed, our previous paper has also shown the good performance of the CAM-Chem model application in eastern China (Wang et al., 2023).

3 Results and discussion

3.1 Exacerbation of O_3 Pollution due to Extreme Weather Conditions

In September 2022, the PRD region experienced continuous extreme weather, resulting in a prolonged period of hot weather conditions. As a consequence, the region encountered 25 consecutive days of regional O_3 pollution (Fig. 1(b)). Monthly O_3 concentrations (MDA8-90 O_3) were situated in high levels reaching up to 92 ppb, approximately 20 ppb higher than the average of the same period during past three years. Meanwhile, the monthly average daily-maximum temperature soared to 32°C, making it the second-highest temperature recorded in September over the past 2 decades (Fig. S5). The extremely high temperature appeared to be a significant driver of O_3 pollution, as evidenced by a high correlation coefficient of 0.70 ($p<0.05$) between O_3 levels and air temperature (Fig. 1(b)). From a synoptic weather perspective, the occurrence of hot weather was the combined effect of multiple tropical cyclones and Western Pacific Subtropical High (WPSH) (Fig. 1(c)). It was recorded that there were four tropical cyclones within the one-month time (2022 September) influenced PRD (described in Table S4). As shown in Fig. 1(c), the combined effects of tropical cyclones and WPSH resulted in the splitting of the subtropical high into two parts. One part lingered over the western Pacific Ocean, while the other remained over the southern region of China, leaving the PRD under the fully control of the mainland high-pressure system. Affected by the sinking air flow under the mainland high, the PRD region experienced conditions characterized by high temperatures, intense solar

radiation, low humidity, and reduced precipitation, creating a favorable environment for photochemical pollution (Fig. 1(d)).

To assess the influence of meteorological parameters on O_3 concentrations, we developed a stepwise regression model to simulate regional O_3 concentrations. By incorporating an extensive range of input variables, including surface and 850hPa meteorological factors, we rigorously tested and identified ten significant factors through T-test analysis. These factors comprised the following: 2m temperature (T2), boundary layer height (BLH), surface relative humidity (RH), surface wind speed (WS), 10m U-component of wind (U10), vertical wind speed (W), 850hPa U-component of wind (U850), total cloud coverage (TCC), 10m V-component of wind (V10), and 850hPa V-component of wind (V850). As illustrated in Fig. 2, meteorological parameters exerted a crucial influence on O_3 concentrations in 2022, surpassing levels in previous years (2019-2021). This underscored the profound impact of meteorology on O_3 pollution. Notably, the factor associated with photochemistry, such as T2, BLH, and RH, played a substantial role, contributing 43.1 ppb, 35.7 ppb, and -9.3 ppb, respectively, to the overall O_3 concentration. In particular, the average daily-maximum air temperature in September maintained at a typically high level (32 °C), which not only accelerated the rates of photochemical reactions, but also stimulated the emission of BVOC from vegetation, thereby exacerbating O_3 concentrations. Furthermore, the increase in BLH and WS compared to previous years indicated relatively favorable ventilation conditions, which facilitated the transport of local and upstream pollutants. Subsequent investigations unveiled that air pollutants from northern regions could be transported to the PRD, contributing to the observed O_3 concentrations (refer to Section 3.3). Additionally, September exhibited relatively dry conditions with lower relative humidity (RH) and less precipitation. Our model revealed a negative correlation between O_3 and RH, suggesting that the presence of water vapor contributed to the photochemical removal of O_3 concentrations (e.g., through HO_x reactions). The reduced RH in September also likely facilitated the persistence of O_3 pollution in the region.

3.2 Weather-boosted BVOC emissions aggravating O_3 production

As one important precursor of O_3 formation, BVOC emissions are sensitive to ambient temperature and solar radiation. Here, we utilized MEGAN model to calculate the regional BVOC emissions. Parallel simulations driven by different meteorological inputs, i.e., meteorological fields in September 2022 and the average meteorological fields in September of the previous three years, were conducted, respectively. It was found that the hot weather in September 2022 led to an increase in BVOC emissions in the PRD region by approximately 10%, relative to that in the same period in the past (Fig. 3(a)). Besides, the in-situ observed isoprene exhibited a significant concentration difference between day and night, i.e., 0.52 – 1.25 ppb during 6:00 – 17:00 and an average of 0.10 ppb at other times (Fig. S6). Not surprisingly, isoprene contributed 7.77 ppb h^{-1} ($\sim$ 40%) to the in-situ net O_3 production rate (OPR) in daytime (Fig. 3(b)). Nevertheless, this was likely a conservative estimate of the biogenic contributions, due to lack of consideration of other biogenic VOC. HCHO, as an important O_3 precursor, is of both anthropogenic and biogenic origin. Here, we utilized WRF-CMAQ simulated biogenic HCHO as input to examine its impact on O_3 formation with F0AM. It was found that biogenic HCHO at an average concentration of 2.46 ppb elevated the OPR by 1.29 ppb h^{-1}. This increased the contribution to OPR of biogenic emissions to 47%. Overall, the modeling results underlined the crucial role of biogenic emissions in building up O_3 levels in September 2022.

Next, we explored the detailed mechanisms of O_3 formation enhancement induced by the rise in isoprene levels due to hot weather (Fig. 4). Simulations were performed for a base case with observations in 2022 and a hypothetical case of lower isoprene levels. We used the ratio of isoprene emissions between 2022 and previous years to scale the observed isoprene in September 2022. So, isoprene in the base case was 10% higher than that in the hypothetical case. HCHO was constrained by the same profile in both cases. It was simulated that the 10% increase in isoprene would lead to an additional O_3 production of 7.5 ppb (OPR of 1.00 ppb h^{-1} at 12:00). While there was little change in the O_3 destruction pathways, the production of NO_2 through RO_2 + NO and HO_2 + NO (pathways leading

to O_3 formation following NO_2 photolysis) increased by 0.63 ppb h^{-1} and 0.38 ppb h^{-1}, respectively. As shown in Fig. 4, this overall effect was caused by multiple reactions involving several generations of isoprene oxidation products/intermediates. The direct oxidation of isoprene by OH and the following transformation from RO_2 through RO to HO_2 only accounted for 30.3% and 42.8% of the increase in total rate of RO_2 + NO and HO_2 production, respectively. The rest was contributed by the degradation of methyl vinyl ketone (MVK) and methacrolein (MACR), two typical isoprene oxidation products (Pierotti et al., 1990). In particular, the formation of peroxyacetyl radical (CH_3CO_3) was enhanced by 0.16 ppb h^{-1}, which further accelerated the rate of RO_2 oxidizing NO by 0.30 ppb h^{-1} (45.6%) and HO_2 production rate by 0.15 ppb h^{-1} (32.5%). Methylglyoxal (MGLYOX) and CH_3CO_3 were the key intermediates in photochemical degradation of MVK and MACR that largely enhanced O_3 formation. The effect of MVK was much more significant than MACR, which was reasonable, due to the presence of a more reactive vinyl group in the MVK molecule.

It is well documented that isoprene emitted from vegetation is highly reactive in the troposphere and is therefore not prone to transport over long distances. Here, we show that the primary oxidation products of isoprene that may be formed during air mass transport (Wang et al., 2022), especially MVK and MACR, make significant contributions to O_3 formation. This presents to be an important mechanism of isoprene contributing to O_3 formation. Hence, the impacts of BVOC oxidation intermediates on downwind air quality warrant more attention (Dreyfus et al., 2002; Lee et al., 2014).

3.3 O_3 enhancement by STE and cross-regional transport

In addition to its influence on meteorological factors and natural emissions, extreme weather can also impact atmospheric transport, modulating the regional air quality. For instance, the STE process is a significant natural process that facilitates the exchange of O_3-rich air from the stratosphere to the troposphere, impacting O_3 levels in the lower atmosphere (Wang et al., 2023). STE often occurs in association with synoptic weather systems such as cyclones, westerly jet stream, frontal activities and troughs of low

pressure (Banerjee et al., 2016). Being affected by the combined influence of the Subtropical High and typhoons, we diagnosed a continuous STE event occurring from September 13, 2022, to September 16, 2022.

Initially, on September 13, a trough of low pressure extended from northwest Inner Mongolia to central China, affecting a large portion of mainland China (Fig. S7). Concurrently, Typhoon "Muifa" developed near the coastline in the western Pacific Ocean, leading to the gradual development of this trough towards the southeastern part of China. On the 15th, the typhoon made landfall in the Yangtze River Delta region. The combined influence of the typhoon's low-pressure center and the external strong anticyclone further extended the trough of low pressure southward (Fig. S7). The dynamic evolution of the weather system facilitated the favorable conditions for cross-regional transport from higher latitudes of China to the lower latitudes, such as the PRD region.

Here, we utilized multiple methods to illustrate the impact of the STE-induced O_3. First of all, we employed potential vorticity (PV) at 300 hPa to distinguish between stratospheric and tropospheric air masses, considering a threshold of 2 potential vorticity units (PVU) as the dynamical tropopause (Li et al., 2023; Wang et al., 2020). According to Fig. 5(a), a notable high value of PV was observed in eastern China, specifically spanning from the North China Plain (NCP) area to southern China on September 14, 2022. This extensive cross-regional transport area is closely associated with typhoon "Muifa" (as depicted in Fig. S5). The presence of a strong anticyclone on the outer periphery of the typhoon further intensified the cross-regional transport in eastern China. This was true with the LPDM simulation, as it revealed that the PRD region was predominantly influenced by northerly air flow originating from central China (Fig. S8). As a result, the potential impact of stratospheric O_3 intrusion on the troposphere formed a distinct and extensive band that stretched from the north to the south over eastern China. The subsequent investigations further supported this finding, as we found similar patterns, including notable high O_3 distribution at 300 hPa (Fig. 5(b)), low specific humidity (Fig. 5(c)), and low geopotential height (Fig. 5(d)) along the high PV area. These patterns suggested that the stratospheric intrusion did

transport both dry and O_3-rich air masses to the troposphere. Meanwhile, the transported region exhibited a prevailing downward airflow with positive vertical velocity (Fig. 5(e)), and a distinct high O_3 area was also observed along the transported band at 700 hPa (Fig. 5(f)), indicating that the O_3 induced by STE could impact the lower troposphere. Similar patterns were consistently observed on other days between September 13-16, 2022 (Fig. S9-S11), confirming the continuous nature of the STE event. The CAM-Chem model was further adopted to quantify the impact of STE-induced O_3. In this model, we introduced a tracer, O_3S, to represent the concentration of O_3 from stratosphere. Fig. 6 convinced again the previous analyses that the transport of O_3-rich air from the stratosphere to the troposphere, spanning from the northern to the southern China. The cross-regional transport of O_3S was notable at higher levels (between 500hPa and 300hPa) in the troposphere with substantial contributions exceeding 50 ppb. Though the influence reduced in the lower of the troposphere, the impacted contribution was still high. The simulated maxima of O_3S at the surface level could reach up to approximately 8 ppb, indicating a non-negligible impact of STE.

4 Conclusion and implication

This study adopted an integrated methodology, utilizing concurrent observations, machine learning techniques, and numerical simulations, to probe how natural processes triggered by extreme hot weather conditions (the continuous combined influence of the Subtropical High and typhoon peripheries) on O_3 pollution. Various natural processes, including meteorological factors, natural emissions, chemistry pathway and atmospheric transport, were investigated and summarized in Fig. 7. Firstly, we found that meteorological conditions during extreme weather events, characterized by high temperatures, high pressure, and low humidity, greatly facilitated regional photochemical reaction. Through the application of machine learning techniques, we identified that meteorological factors contribute an additional 10.8 ppb to O_3 levels compared to the same period in previous years, with surface temperature exerting the most prominent influence. Furthermore, our investigation revealed that the hot weather stimulated BVOC emissions (increased by

10%). Due to the typical high NO_x environment (mainly from anthropogenic emission) in the PRD region, BVOC emissions aggravated photochemical reaction and contributed nearly half of in-situ O_3 production. The chemical transformation pathways of isoprene and its intermediate products were further explored, it was found that the further degradation of initial oxidation products of isoprene was responsible for a large fraction of isoprene contributions to O_3 formation. This could be an important mechanism of isoprene affecting downwind air quality. In addition, the impact of extreme weather on atmospheric transport was also investigated. The phenomenon of STE usually takes place in high latitudes. Interestingly, we discovered that the outer periphery of a typhoon, aggravated the cross-regional transport of STE-induced O_3, spanning from the northern China to southern China. This process resulted in a non-negligible contributor to the surface levels in downwind area (such as the PRD, reached a maximum of ~ 8 ppb).

Our study underscores the importance of natural processes induced by extreme weather events in O_3 pollution and provides valuable insights for future endeavors in O_3 pollution control. Given the impact of climate change, many regions around the world are experiencing an increase in the frequency of extreme weather events, thereby intensifying natural processes. This trend is particularly notable in developed regions with high levels of anthropogenic emissions, such as eastern China, southeastern America and northern India. The interaction between natural process and human activities might further exacerbate air pollution. Future pollution control and prevention efforts should not solely focus on reducing anthropogenic emissions. Instead, a comprehensive consideration of both anthropogenic impact and natural impact should be taken into account, and a coordinated cross-regional joint emission control is highly recommended.
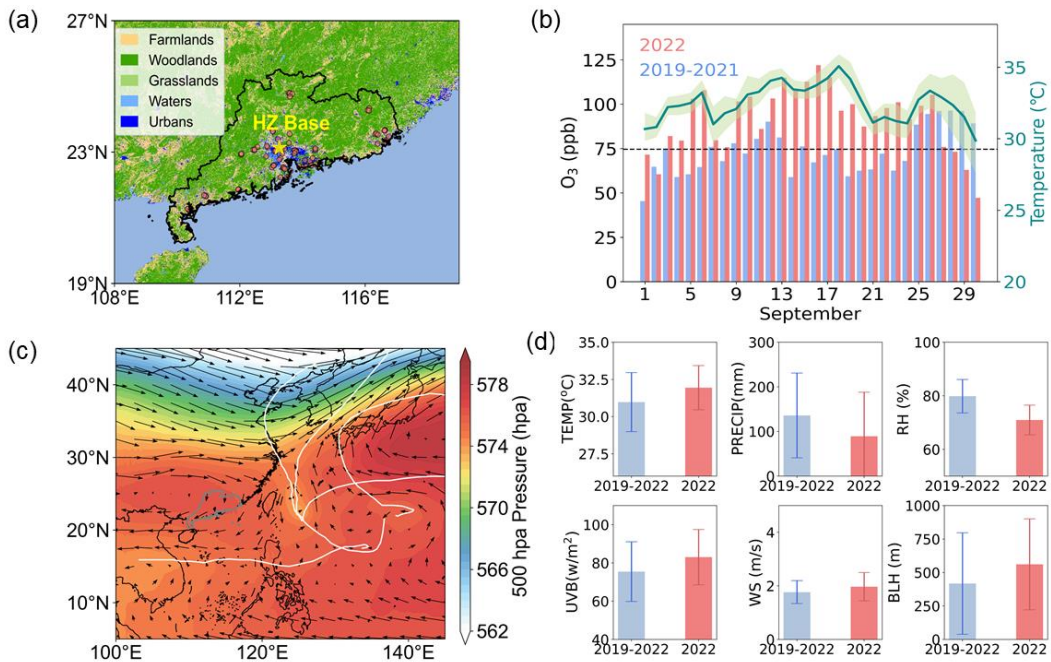
Figure 1 (a) Map showing the geographical distribution of PRD. The dots show the air quality monitoring network and the yellow star shows the in-situ site at Guangzhou Haizhu Urban Ecological Meteorological Comprehensive Observation Base (HZ Base); (b) Variation of MDA8-90 O_3 concentrations and regional daily max temperature (The green line shows the average, and the upper and lower shade indicate the 75th and 25th percentile, respectively); (c) Distribution of 500 hPa pressure and winds of September 2022. The white line shows the typhoon track; (d) Comparisons of meteorological parameters (temperature (TEMP), precipitation (PRECIP), relative humidity (RH), ultraviolet radiation b (UVB), wind speed (WS) and boundary layer height (BLH)) between 2022 and 2019-2021
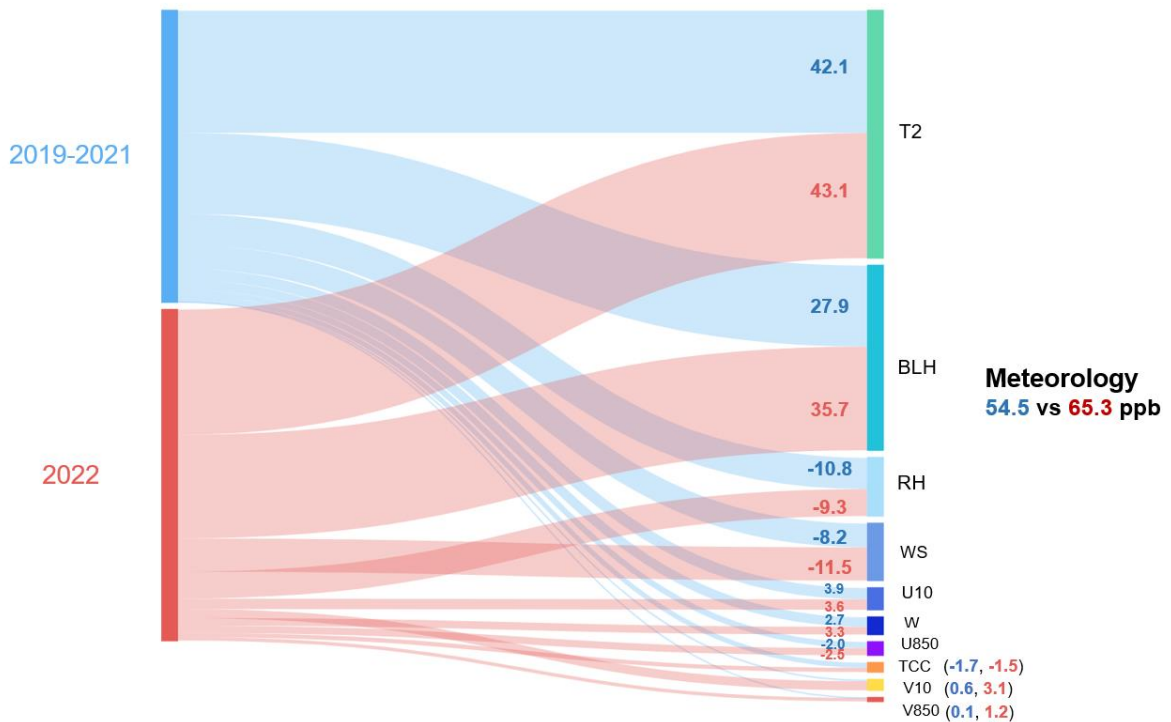
Figure 2 Contributions of multi-meteorological factors (2m temperature (T2), boundary layer height (BLH),

relative humidity (RH), wind speed (WS), 10 m u-component of wind (U10), w (vertical wind speed), 850 hPa u-

544
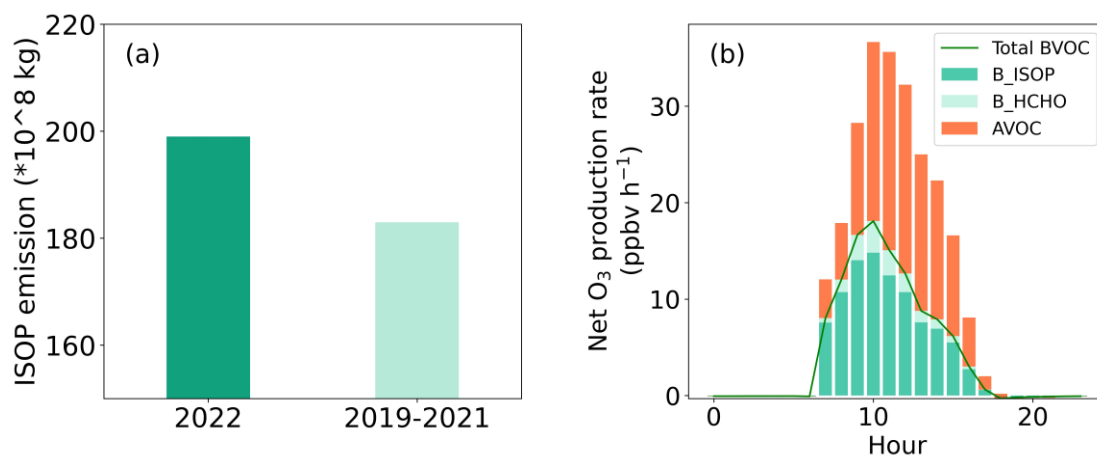
Figure 3 (a) Isoprene emissions in PRD in September in 2022 and 2019 – 2021; (b) Net OPR attributed to biogenic isoprene (B_ISOP), biogenic HCHO (B_HCHO), total BVOC and anthropogenic VOC (AVOC) in September 2022.

547

548

549
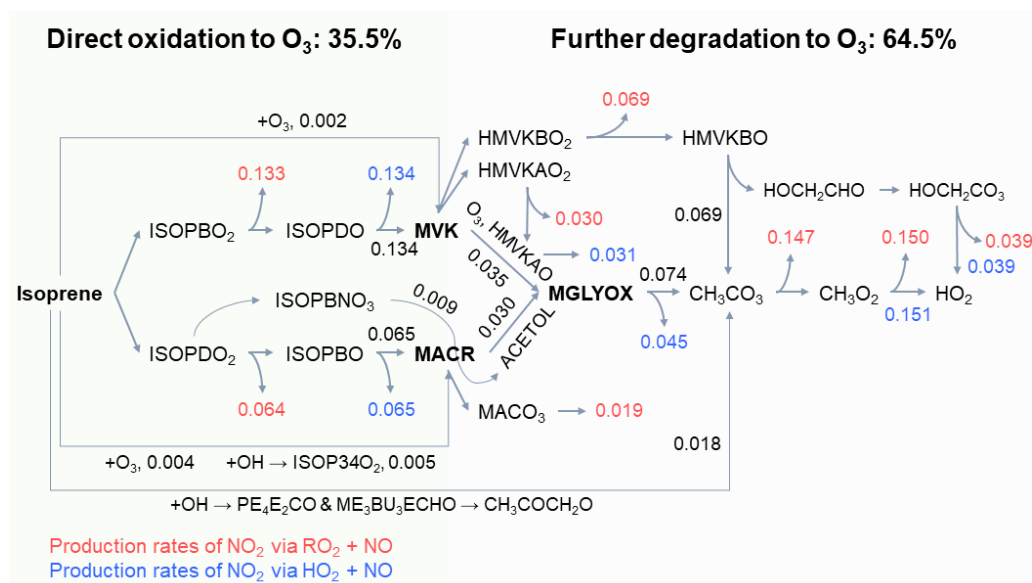
Figure 4 Changes in the rates (numbers; unit: ppbv h^{-1}) of major reactions leading to O₃ formation at 12:00 induced by 10% increase in isoprene concentrations. Red and blue fonts indicate the production rates of NO₂ via RO₂ + NO and HO₂ + NO, respectively. Abbreviations of the species conform to the MCM naming convention (http://chmlin9.leeds.ac.uk/MCMv3.3.1/home.htt).

554

555

556
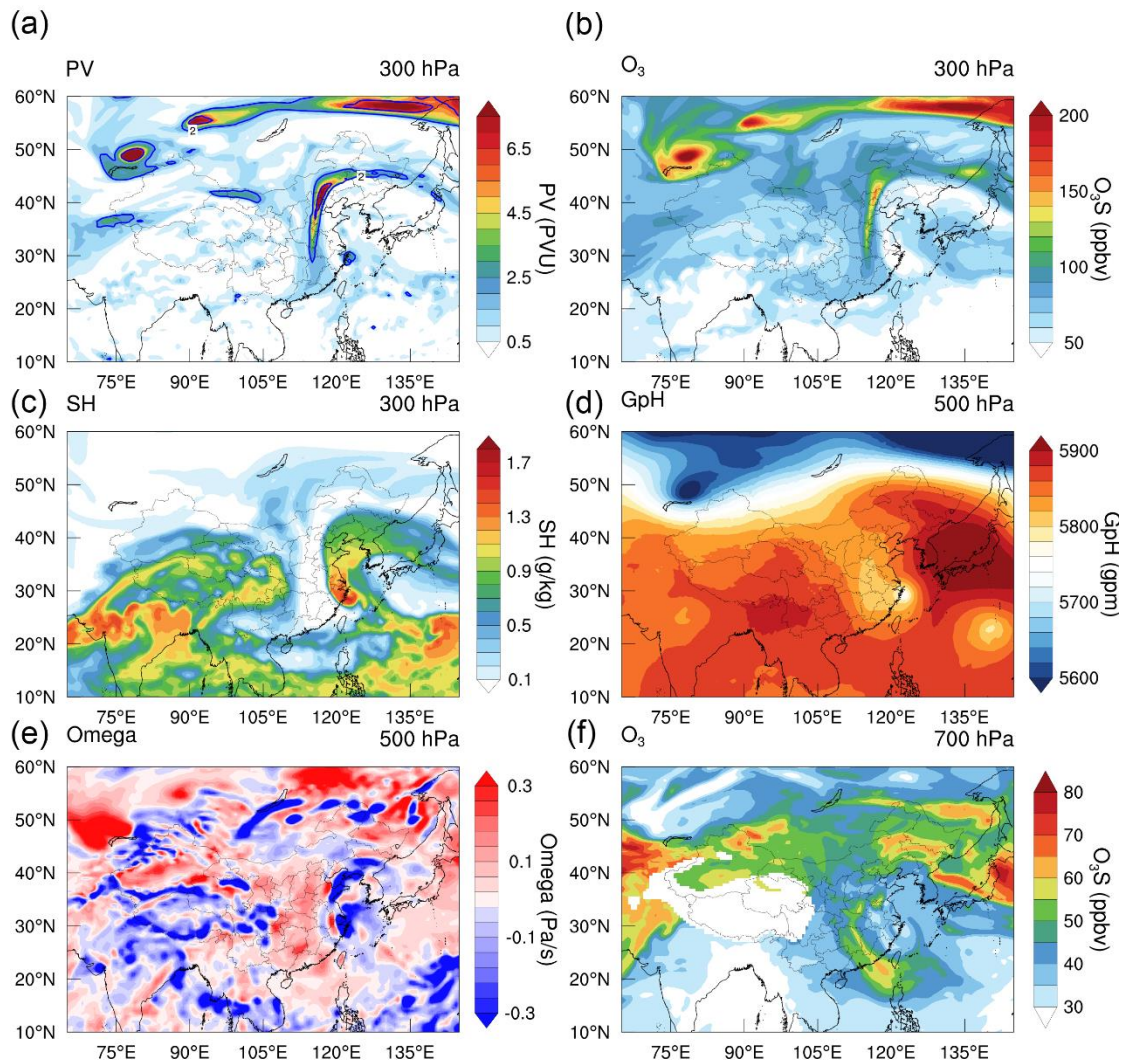
557

558 Figure 5 Evidence illustrating STE O_3 intrusion on September 14, 2022. (a) Spatial distribution of potential vorticity

559 (PV) at 300hPa over China (The blue solid line indicates the dynamical tropopause of 2PVU, 1 PVU=10^{-6} m^2 s^{-1} K

560 kg-1); (b-e) The distribution of O_3 concentration (at 300 hPa), specific humidity (at 300 hPa, SH), geopotential height

561 (at 500 hPa, Gph), vertical velocity (at 500 hPa, Omega), and O_3 concentration (at 700 hPa), respectively. All the

562 data were identified based on ERA5 database.

563

564

565

566

567
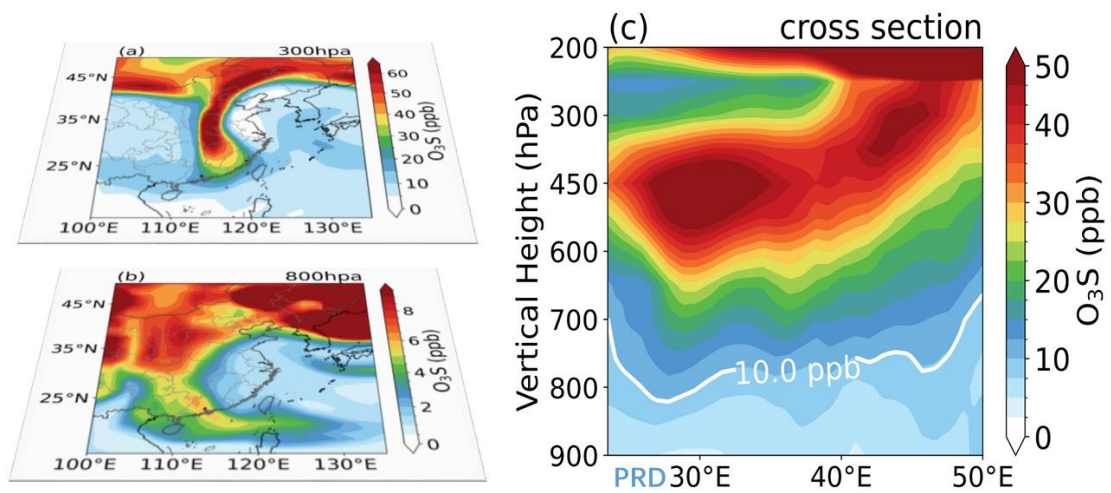
568

569 Figure 6 Distribution of CAM-chem simulated O_3S. (a) O_3S distribution at 300 hPa; (b) same as (a) but at 800 hPa;

570 (c) Vertical transection of O_3S along the 113°E.

571

572
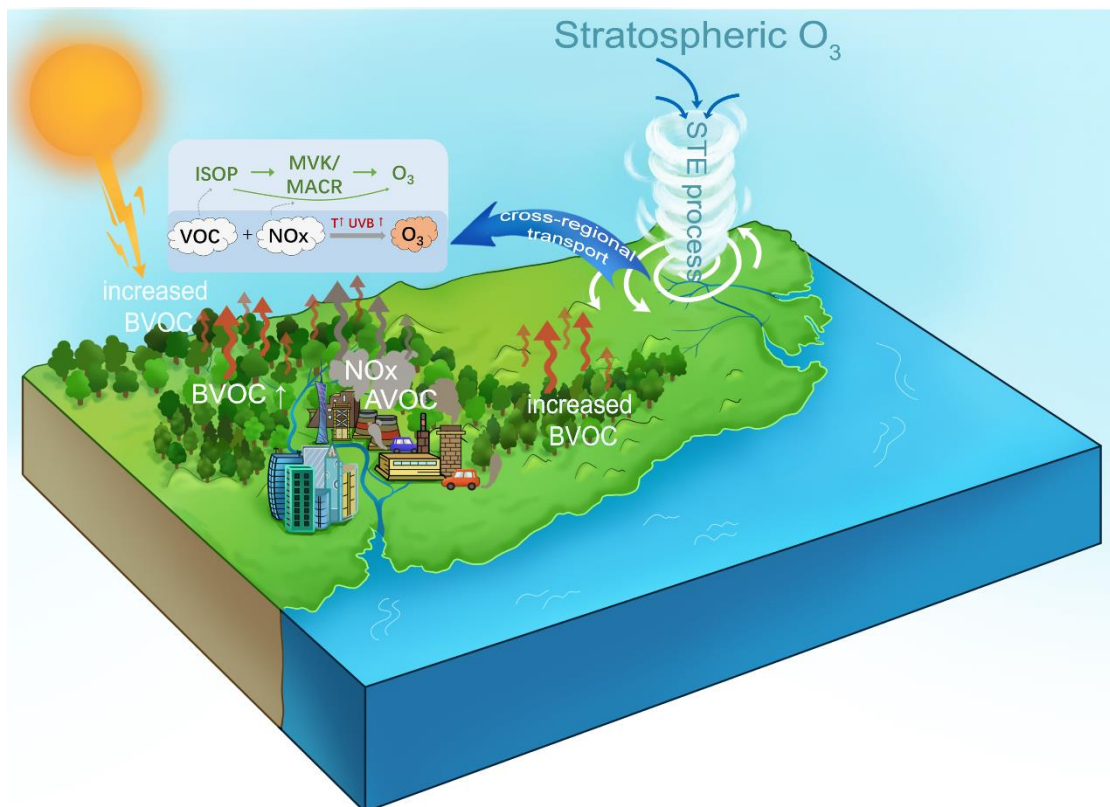
573

574 Figure 7 Conceptual scheme illustrating how extreme weather induced natural processes affecting O3 in PRD. ISOP,

575 MVK and MACR refer to isoprene, methyl vinyl ketone and methacrolein, respectively.

576

Associated Content (Supporting Information)

Validation of the stepwise regression model(Fig. S1); Synoptic weather distribution (Fig. S2); LPDM simulated 48h retroplume (footprint residence time) (Fig. S3); Evidence illustrating STE O3 intrusion (Fig. S4-S6); Introduction of monitoring instruments (Table S1); Introduction of the recorded tropical cyclones (Table S2)

Author Contributions

N.W. designed the research. N.W. and X.L. wrote the manuscript. N.W. , X.L., H.W., X.C. and F.Y. contributed to the interpretation of the results. All authors provided critical feedback and helped shape the research, analysis, and manuscript.

Competing Interests

The contact author has declared that none of the authors has any competing interests.

Code/Data availability

The code and data used in this study are available upon request from Nan Wang (nan.wang@scu.edu.cn) and Xiaopu Lyu (xiaopu_lyu@hkbu.edu.hk)

Acknowledgement

This study is funded by Fundamental Research Funds for the Central Universities (Grant No. YJ202313), the Guangdong Basic and Applied Basic Research Foundation (Grant No. 2022A1515011753, and 2023A1515012205), the Science and Technology Research Project of Guangdong Meteorological Bureau (Grant No. GRMC2020Z06), and the Young Talent Support Project of Guangzhou Association for Science and Technology (Grant No. QT-2023-048).

Reference

Ashmore, M.: Assessing the future global impacts of ozone on vegetation, Plant, Cell & Environment, 28, 949-964, 2005.

Banerjee, A., Maycock, A. C., Archibald, A. T., Abraham, N. L., Telford, P., Braesicke, P., and Pyle, J. A.: Drivers of changes in stratospheric and tropospheric ozone between year 2000 and 2100, Atmospheric Chemistry and Physics, 16, 2727-2746, 2016.

Briegleb, B., Minnis, P., Ramanathan, V., and Harrison, E.: Comparison of regional clear-sky albedos inferred from satellite observations and model computations, Journal of Applied Meteorology and Climatology, 25, 214-226, 1986.

Camalier, L., Cox, W., and Dolwick, P.: The effects of meteorology on ozone in urban areas and their use in assessing ozone trends, Atmospheric environment, 41, 7127-7137, 2007.

Chan, C. and Chan, L.: Effect of meteorology and air pollutant transport on ozone episodes at a subtropical coastal Asian city, Hong Kong, Journal of Geophysical Research: Atmospheres, 105, 20707-20724, 2000.

Chen, X., Wang, N., Wang, G., Wang, Z., Chen, H., Cheng, C., Li, M., Zheng, L., Wu, L., Zhang, Q., Tang, M., Huang, B., Wang, X., and Zhou, Z.: The Influence of Synoptic Weather Patterns on Spatiotemporal Characteristics of Ozone Pollution Across Pearl River Delta of Southern China, Journal of Geophysical Research: Atmospheres, 127, 10.1029/2022jd037121, 2022.

De Smedt, I., Stavrakou, T., Müller, J. F., Van Der A, R., and Van Roozendael, M.: Trend detection in satellite observations of formaldehyde tropospheric columns, Geophysical Research Letters, 37, 2010.

Derwent, R. G., Jenkin, M. E., Saunders, S. M., and Pilling, M. J.: Photochemical ozone creation potentials for organic compounds in northwest Europe calculated with a master chemical mechanism, Atmospheric environment, 32, 2429-2441, 1998.

Ding, A., Huang, X., and Fu, C.: Air pollution and weather interaction in East Asia, in: Oxford Research Encyclopedia of Environmental Science, 2017.

Dreyfus, G. B., Schade, G. W., and Goldstein, A. H.: Observational constraints on the contribution of isoprene oxidation to ozone production on the western slope of the Sierra Nevada, California, Journal of Geophysical Research: Atmospheres, 107, ACH 1-1-ACH 1-17, 2002.

Eyring, V., Arblaster, J. M., Cionni, I., Sedláček, J., Perlwitz, J., Young, P. J., Bekki, S., Bergmann, D., Cameron-Smith, P., and Collins, W. J.: Long-term ozone changes and associated climate impacts in CMIP5 simulations, Journal of Geophysical Research: Atmospheres, 118, 5029-5060, 2013.

Gao, D., Xie, M., Liu, J., Wang, T., Ma, C., Bai, H., Chen, X., Li, M., Zhuang, B., and Li, S.: Ozone variability induced by synoptic weather patterns in warm seasons of 2014–2018 over the Yangtze River Delta region, China, Atmospheric Chemistry and Physics, 21, 5847-5864, 2021.

Gaudel, A., Cooper, O. R., Ancellet, G., Barret, B., Boynard, A., Burrows, J. P., Clerbaux, C., Coheur, P.-F., Cuesta, J., and Cuevas, E.: Tropospheric Ozone Assessment Report: Present-day distribution and trends of tropospheric ozone relevant to climate and global atmospheric chemistry model evaluation, Elementa: science of the anthropocene, 6, 2018.

Guenther, A., Jiang, X., Heald, C. L., Sakulyanontvittaya, T., Duhl, T. a., Emmons, L., and Wang, X.: The Model of Emissions of Gases and Aerosols from Nature version 2.1 (MEGAN2. 1): an extended and updated framework for modeling biogenic emissions, Geoscientific Model Development, 5, 1471-1492, 2012.

Han, H., Liu, J., Shu, L., Wang, T., and Yuan, H.: Local and synoptic meteorological influences on

daily variability in summertime surface ozone in eastern China, Atmospheric Chemistry and Physics, 20, 203-222, 2020.

Jacob, D. J.: Heterogeneous chemistry and tropospheric ozone, Atmospheric Environment, 34, 2131-2159, 2000.

Jenkin, M. E. and Clemitshaw, K. C.: Ozone and other secondary photochemical pollutants: chemical processes governing their formation in the planetary boundary layer, Atmospheric Environment, 34, 2499-2527, 2000.

Johnsson, T.: A procedure for stepwise regression analysis, Statistical Papers, 33, 21-29, 1992.

Knowlton, K., Rosenthal, J. E., Hogrefe, C., Lynn, B., Gaffin, S., Goldberg, R., Rosenzweig, C., Civerolo, K., Ku, J.-Y., and Kinney, P. L.: Assessing ozone-related health impacts under a changing climate, Environmental health perspectives, 112, 1557-1563, 2004.

Lee, K.-Y., Kwak, K.-H., Ryu, Y.-H., Lee, S.-H., and Baik, J.-J.: Impacts of biogenic isoprene emission on ozone air quality in the Seoul metropolitan area, Atmospheric Environment, 96, 209-219, 2014.

Lei, Y., Yue, X., Liao, H., Zhang, L., Zhou, H., Tian, C., Gong, C., Ma, Y., Cao, Y., and Seco, R.: Global perspective of drought impacts on ozone pollution episodes, Environmental science & technology, 56, 3932-3940, 2022.

Li, T., Wu, N., Chen, J., Chan, P.-w., Tang, J., and Wang, N.: Vertical exchange and cross-regional transport of lower-tropospheric ozone over Hong Kong, Atmospheric Research, 292, 106877, 10.1016/j.atmosres.2023.106877, 2023.

Lu, X., Zhang, L., and Shen, L.: Meteorology and Climate Influences on Tropospheric Ozone: a Review of Natural Sources, Chemistry, and Transport Patterns, Current Pollution Reports, 5, 238-260, 10.1007/s40726-019-00118-3, 2019.

Lu, X., Hong, J., Zhang, L., Cooper, O. R., Schultz, M. G., Xu, X., Wang, T., Gao, M., Zhao, Y., and Zhang, Y.: Severe surface ozone pollution in China: a global perspective, Environmental Science & Technology Letters, 5, 487-494, 2018.

Lyu, X., Guo, H., Zou, Q., Li, K., Xiong, E., Zhou, B., Guo, P., Jiang, F., and Tian, X.: Evidence for Reducing Volatile Organic Compounds to Improve Air Quality from Concurrent Observations and In Situ Simulations at 10 Stations in Eastern China, Environmental Science & Technology, 56, 15356-15364, 2022.

Lyu, X., Li, K., Guo, H., Morawska, L., Zhou, B., Zeren, Y., Jiang, F., Chen, C., Goldstein, A. H., and Xu, X.: A synergistic ozone-climate control to address emerging ozone pollution challenges, One Earth, 6, 964-977, 2023.

Lyu, X., Wang, N., Guo, H., Xue, L., Jiang, F., Zeren, Y., Cheng, H., Cai, Z., Han, L., and Zhou, Y.: Causes of a continuous summertime O 3 pollution event in Jinan, a central city in the North China Plain, Atmospheric Chemistry and Physics, 19, 3025-3042, 2019.

Pierotti, D., Wofsy, S., Jacob, D., and Rasmussen, R.: Isoprene and its oxidation products: Methacrolein and methyl vinyl ketone, Journal of Geophysical Research: Atmospheres, 95, 1871-1881, 1990.

Povey, A. and Grainger, R.: Known and unknown unknowns: uncertainty estimation in satellite remote sensing, Atmospheric Measurement Techniques, 8, 4699-4718, 2015.

Pusede, S. E., Steiner, A. L., and Cohen, R. C.: Temperature and recent trends in the chemistry of continental surface ozone, Chemical reviews, 115, 3898-3918, 2015.

Stohl, A., Bonasoni, P., Cristofanelli, P., Collins, W., Feichter, J., Frank, A., Forster, C., Gerasopoulos, E., Gäggeler, H., and James, P.: Stratosphere-troposphere exchange: A review, and what we have

693 learned from STACCATO, Journal of Geophysical Research: Atmospheres, 108, 2003.

694 Wang, H., Wang, W., Shangguan, M., Wang, T., Hong, J., Zhao, S., and Zhu, J.: The Stratosphere-

695 to-Troposphere Transport Related to Rossby Wave Breaking and Its Impact on Summertime

696 Ground-Level Ozone in Eastern China, Remote Sensing, 15, 2647, 10.3390/rs15102647, 2023.

697 Wang, N., Huang, X., Xu, J., Wang, T., Tan, Z.-m., and Ding, A.: Typhoon-boosted biogenic emission

698 aggravates cross-regional ozone pollution in China, Science Advances, 8, eabl6166, 2022.

699 Wang, N., Lyu, X., Deng, X., Huang, X., Jiang, F., and Ding, A.: Aggravating O3 pollution due to

700 NOx emission control in eastern China, Science of the Total Environment, 677, 732-744, 2019.

701 Wang, T., Xue, L., Brimblecombe, P., Lam, Y. F., Li, L., and Zhang, L.: Ozone pollution in China: A

702 review of concentrations, meteorological influences, chemical precursors, and effects, Science of

703 the Total Environment, 575, 1582-1596, 2017.

704 Wang, Y., Wang, H., and Wang, W.: A stratospheric intrusion-influenced ozone pollution episode

705 associated with an intense horizontal-trough event, Atmosphere, 11, 164, 2020.

706 Westerling, A. L., Hidalgo, H. G., Cayan, D. R., and Swetnam, T. W.: Warming and earlier spring

707 increase western US forest wildfire activity, science, 313, 940-943, 2006.

708 Yue, X. and Unger, N.: Fire air pollution reduces global terrestrial productivity, Nature

709 Communications, 9, 5413, 2018.

710 Zou, Y., Deng, X., Zhu, D., Gong, D., Wang, H., Li, F., Tan, H., Deng, T., Mai, B., and Liu, X.:

711 Characteristics of 1 year of observational data of VOCs, NO x and O 3 at a suburban site in

712 Guangzhou, China, Atmospheric Chemistry and Physics, 15, 6625-6636, 2015.

713

714